FULL PAPER

ADVANCED
FUNCTIONAL
MATERIALS
www.afm-journal.d

Check for updates

Self-Powered Flexible TiO$_2$ Fibrous Photodetectors: Heterojunction with P3HT and Boosted Responsivity and Selectivity by Au Nanoparticles

Lingxia Zheng,* Xiaolei Deng, Yongzhi Wang, Jiaxin Chen, Xiaosheng Fang,* Liang Wang, Xiaowei Shi, and Huajun Zheng*

A novel inorganic–organic heterojunction (TiO$_2$/P3HT (poly(3-hexylthiophene)) is easily prepared by a combination of anodization and vacuumed dip-coating methods, and the constructed flexible fibrous photodetector (FPD) exhibits high-performance self-powered UV–visible broadband photoresponse with fast speed, high responsivity, and good stability, as well as highly stable performance at bending states, showing great potential for wearable electronic devices. Moreover, Au nanoparticles are deposited to further boost the responsivity and selectivity by regulating the sputtering intervals. The optimal Au/TiO$_2$/P3HT FPD yields an ≈700% responsivity enhancement at 0 V under 350 nm illumination. The sharp cut-off edge and high UV–visible rejection ratio (≈17 times higher) indicate a self-powered flexible UV photodetector. This work provides an effective and versatile route to modulate the photoelectric performance of flexible electronic devices.

1. Introduction

Flexible/wearable electronic devices that can be conformably and comfortably attached to human body have raised worldwide interest for the applications in monitoring personal health conditions and environmental changes in real time with wireless communications,[1] which involves smart skins,[2,3] wristbands,[4] lenses,[5] helmets,[6] textiles,[7,8] etc. Fiber electronic devices have become an important part, which can be easily woven into cloth assisted by traditional weaving technique. Recently,

flexible fibrous photodetectors (FPDs) have attracted huge attention because of their promising applications in portable devices, aerospace science and civil engineering, which requires flexibility, lightweight, shock-resistance, and softness.[9–14] Generally, "5S" key parameters:[15] sensitivity, selectivity, speed, stability and signal-to-noise ratio, are used to evaluate the optoelectronic performance of traditional photodetectors (PDs). When it comes to flexible FPDs, more features need to be considered, such as portability, flexibility, and strength because they will greatly influence photodetection properties under mechanical stress.[1] One of the critical issue is to develop intimate and robust interface between the fibrous substrate and photoactive material to ensure stable performance during device deformation, as well as the enhanced performance competitive with their planar counterparts.[14,16–20] Particularly, metal fiber substrate is reported to be the most extensively used type, which not only serves as an electrode but also the precursor material for in situ growth of photoactive nanostructures, endowing good flexibility and mechanical performance.

To meet the evolution of modern electronics in the trends of being miniature, energy saving, portable, and zero-maintenance, self-powered FPDs without consuming an external power source (e.g., batteries) are greatly urgent.[21–25] Briefly, there are two general routes to realize self-powered FPDs in the viewpoint of energy conversion.[26,27] One route is to integrate FPDs with miniaturized energy-harvesting/storage components like nanogenerators, solar cells, and supercapacitors,[28–30] which transforms light signals into electricity along with mechanical energy or chemical energy at the expense of increased complexity and cost. The other is to exploit photodiodes through construction of Schottky junction, p-n junctions and heterojunctions due to the efficient separation ability of photogenerated electron–hole pairs by the photovoltaic effect, which directly transforms light signals into electronic ones.[9,10] Only several attempts have been made to fabricate flexible fiber-shaped photodetectors with self-powered mode. For example, Zeng et. al.[9] reported a self-powered ZnO based fiber-shaped omnidirectional UV PD with an on/off ratio of ≈2, responsivity of 9.96 mA W^{-1} at 350 nm. Xu et. al.[10] reported a novel self-powered TiO$_2$/CuZnS wearable FPD with high spectral

Dr. L. X. Zheng, X. L. Deng, Y. Z. Wang, Prof. L. Wang Dr. X. W. Shi, Prof. H. J. Zheng
State Key Laboratory Breeding Base of Green Chemistry Synthesis Technology
Zhejiang University of Technology
Hangzhou 310032, P. R. China
E-mail: lxzheng@zjut.edu.cn; zhenghj@zjut.edu.cn
Dr. L. X. Zheng, X. L. Deng, Y. Z. Wang, Dr. X. W. Shi, Prof. H. J. Zheng
Department of Applied Chemistry
Zhejiang University of Technology
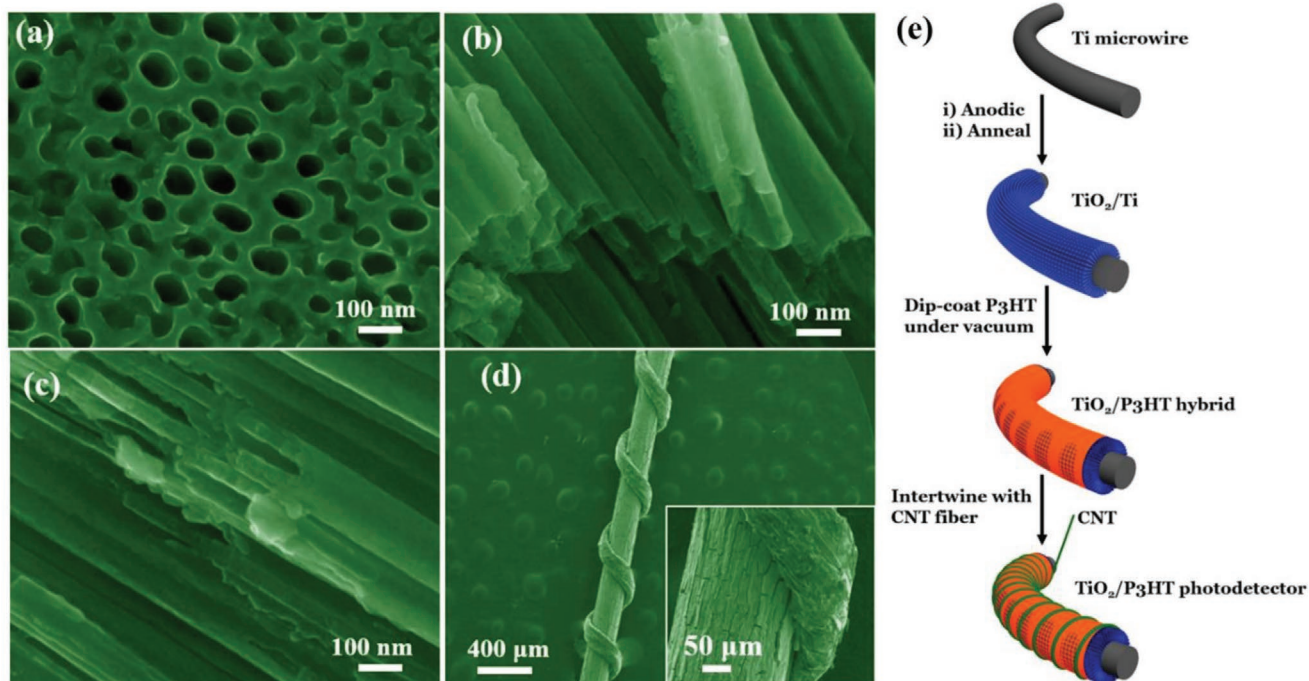Hangzhou 310032, P. R. China
Dr. L. X. Zheng, J. X. Chen, Prof. X. S. Fang
Department of Materials Science
Fudan University
Shanghai 200433, P. R. China
E-mail: xshfang@fudan.edu.cn

The ORCID identification number(s) for the author(s) of this article can be found under https://doi.org/10.1002/adfm.202001604.

Figure 1. a) Top-surface and b,c) lateral scanning electron microscopy (SEM) images of TiO_2/P3HT hybrid. d) SEM image of TiO_2/P3HT fibrous device. Inset shows the magnification. e) Illustration of the preparation process of TiO_2/P3HT FPD.

selectivity and high responsivity (UV–visible rejection ratio of 11.6; 2.54 mA W^{-1} at 0 V under 300 nm UV light). Li et. al.[31] presented a flexible double-twisted broadband perovskite PD based on two fiber substrates with an ultrahigh detectivity at zero bias. Considering the crooked and limited illumination area of photoactive material on fibrous substrates, it is challenge to generate decent photocurrent/responsivity and desirable sensitivity without an external power source. Besides, it is still costly and sophisticated to fabricate high quality junctions, thus hindering the practical utilization. Therefore, it would be of great advantages to develop novel junction flexible fibrous PDs with self-powered property via a low-cost and facile strategy.

Inorganic-organic hybrid heterojunctions afford a promising way by combining the excellent intrinsic carrier mobility of inorganic materials and the abundant merits of organic components with tunable functionality, easy of fabrication, low cost and high flexibility.[23,24,32–35] P3HT is a typical π-electron conjugated polymer with a high hole-transport rate and strong visible light absorption, which has been widely applied in photovoltaic devices owing to the semiconductivity and high stability.[32,33,36] Among the inorganic semiconductors, anodic TiO_2 nanotubes (TiO_2NTs) array standing vertically on the surface of Ti metal is a promising candidate to construct high-performance self-powered PDs in the viewpoint of high surface-to-volume ratio, well-defined charge transfer pathway and good adhesion to Ti metal substrate, leading to good photosensitivity, high responsivity and excellent stability.[10,37–39] In this regard, highly ordered 1D TiO_2NTs are in situ grown on the surface of Ti microwire to ensure the intimate contact between the oxide and Ti electrode. The uniform loading of P3HT is through a vacuumed dip-coating method in order to

better engineer the p-n interface, making it reside on the tube mouths and intertubular gaps instead of innertubes. The constructed TiO_2/P3HT FPD employing carbon nanotubes (CNT) yarn intertwined around the photoactive materials as the other electrode (**Figure 1**e) demonstrates high performance self-powered flexible UV–visible broadband photodetection. Interestingly, the responsivity and selectivity can be easily regulated by Au nanoparticles (AuNPs) decoration using an ion-sputtering method, which enables a high-performance self-powered flexible UV photodetector.

2. Results and Discussion

The structural morphologies of TiO_2/P3HT hybrid and TiO_2NTs array on fibrous substrates are presented in Figure 1 and Figure S1, Supporting Information. Highly-ordered 1D TiO_2NTs are radically formed and standing vertically to the surface of Ti microwire by a conventional two-step anodization method. The length of TiO_2NTs array is ≈6 µm with outer tube diameters ranging from 100 to 145 nm. Top-opened tubular morphology with very clean surface is observed, providing easy access for subsequent loading. After using a vacuumed dip-coating method, conducting polymer P3HT is introduced which covers both the tube-mouths and the outer tube-walls of TiO_2NTs (Figure 1a–c). It is noteworthy that benefitted from the well-permeation of organic precursor solution into the inter-tubular gaps induced by the strong capillary force under vacuum condition, a thin layer of P3HT is formed at the outer tube walls of TiO_2NTs with the hollow tube channels unchanged, which not only promises good contact between n-type TiO_2 and p-type P3HT to construct built-in electric field, but also retaining

porous architecture and vertical transmission pathway to facilitate effective carrier transfer. The existence and distribution of element sulfur (S) in SEM-EDS (X-Ray Energy Dispersive Spectroscopy) mapping images in Figure S2, Supporting Information also confirm the uniform distribution of P3HT along with the tubes. The fibrous PD device structure and preparation scheme are shown in Figure 1d,e, respectively. The CNT yarn was twisted tightly and winded around the Ti-TiO$_2$/P3HT microwire, and the extended part acted as the outer electrode. The other end of the Ti metal fiber was polished and acted as the inner electrode. The inset image (Figure 1d) reveals the intimate contact between the CNT electrode and photoactive materials without gaps, which is highly desirable for good charge collection efficiency.

Transmission electron microscopy (TEM) and high resolution TEM (HRTEM) images are examined to reveal more structural information of TiO$_2$/P3HT hybrid as shown in **Figure 2**. Figure 2a,b show the hollow nanotubes array with inner diameters of 50–70 nm and wall thickness of 20–35 nm. The elemental mapping images in Figure 2c also verify the presence and location of P3HT, agreeing well with the scanning electron microscopy (SEM) results (Figure 1 and Figure S2, Supporting Information). HRTEM images (Figure 2d,e) reveal the amorphous nature of P3HT layer with thickness of 13–20 nm. The distinct lattice fringes with a distance of 0.354 nm correspond to the (101) plane of anatase TiO$_2$.

The X-ray diffraction (XRD) patterns of TiO$_2$/P3HT hybrid and pure TiO$_2$NTs sample are displayed in **Figure 3**a. All the diffraction peaks can be assigned to anatase TiO$_2$ (JCPDS 21-1272) and metallic Ti wire (JCPDS 44-1294) in the pure TiO$_2$NTs sample. For TiO$_2$/P3HT hybrid, only two diffraction peaks located at 25.3° and 48.1° can be assigned to the (101) and (200) planes of anatase TiO$_2$ while no obvious signals for P3HT can be detected, which is possibly because the much lower amount of P3HT is below the equipment detection limit. Therefore, in order to verify the presence of P3HT in the composite, Raman spectroscopy was performed under an excitation wavelength of 532 nm. Figure 3b shows the Raman spectrum of pure TiO$_2$NTs with a dominant peak at 145 cm^{-1} due to the O-Ti-O symmetric E_g anatase vibration mode. Three characteristic peaks at 395 (B_{1g}), 515 (A_{1g}), and 638 cm^{-1} (E_g) also confirm the anatase phase of TiO$_2$ and in consistent with the XRD results (Figure 3a).[40] For TiO$_2$/P3HT hybrid, except the dominant peak assigning to anatase TiO$_2$ (E_g), two characteristic bands at 1380 and 1445 cm^{-1} are assigned to the symmetric stretching modes of the C=C and C−C intra-ring bonds, respectively, which also verifies the existence of P3HT.[41]

The electrical and photodetection properties of TiO$_2$/P3HT based fibrous photodetector (FPD) were systematically investigated by a two-probe method under ambient condition and monochromatic illumination, and the results are shown in **Figure 4**. The current–voltage ($I–V$) curve under dark implies
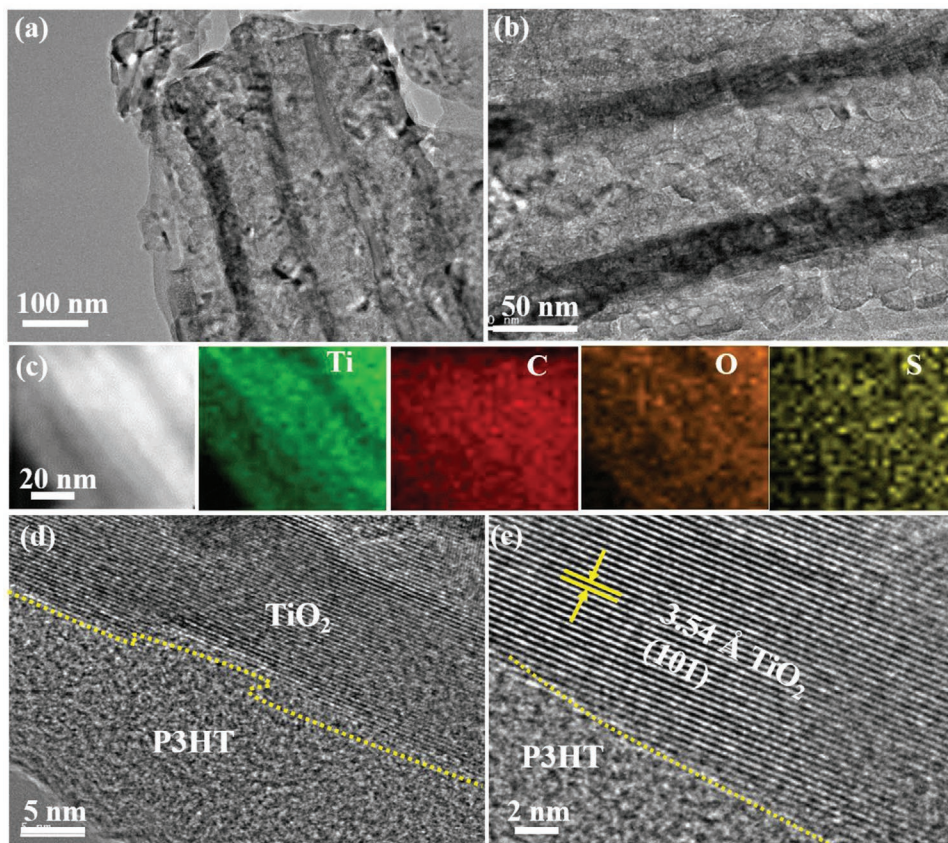
Figure 2. a,b) TEM images of TiO$_2$/P3HT hybrid. c) TEM-EDS mapping showing the elemental distribution of Ti, C, O, and S. d,e) HRTEM images of TiO$_2$/P3HT hybrid.
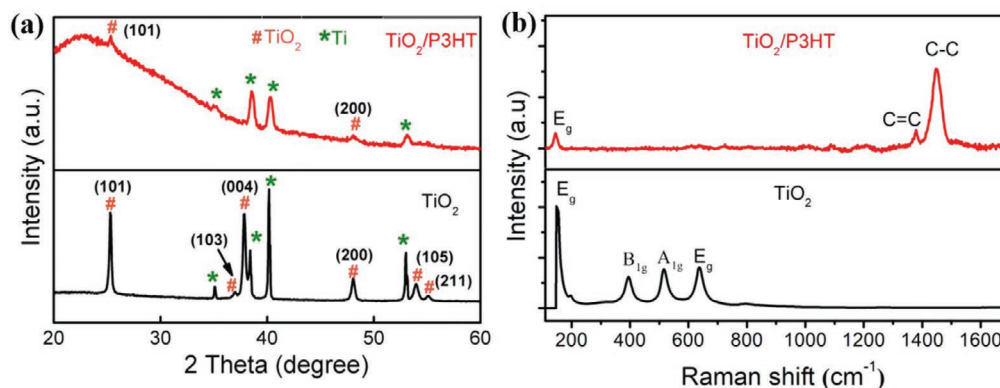
Figure 3. a) XRD patterns and b) Raman spectra of pure TiO_2NTs and TiO_2/P3HT hybrid.

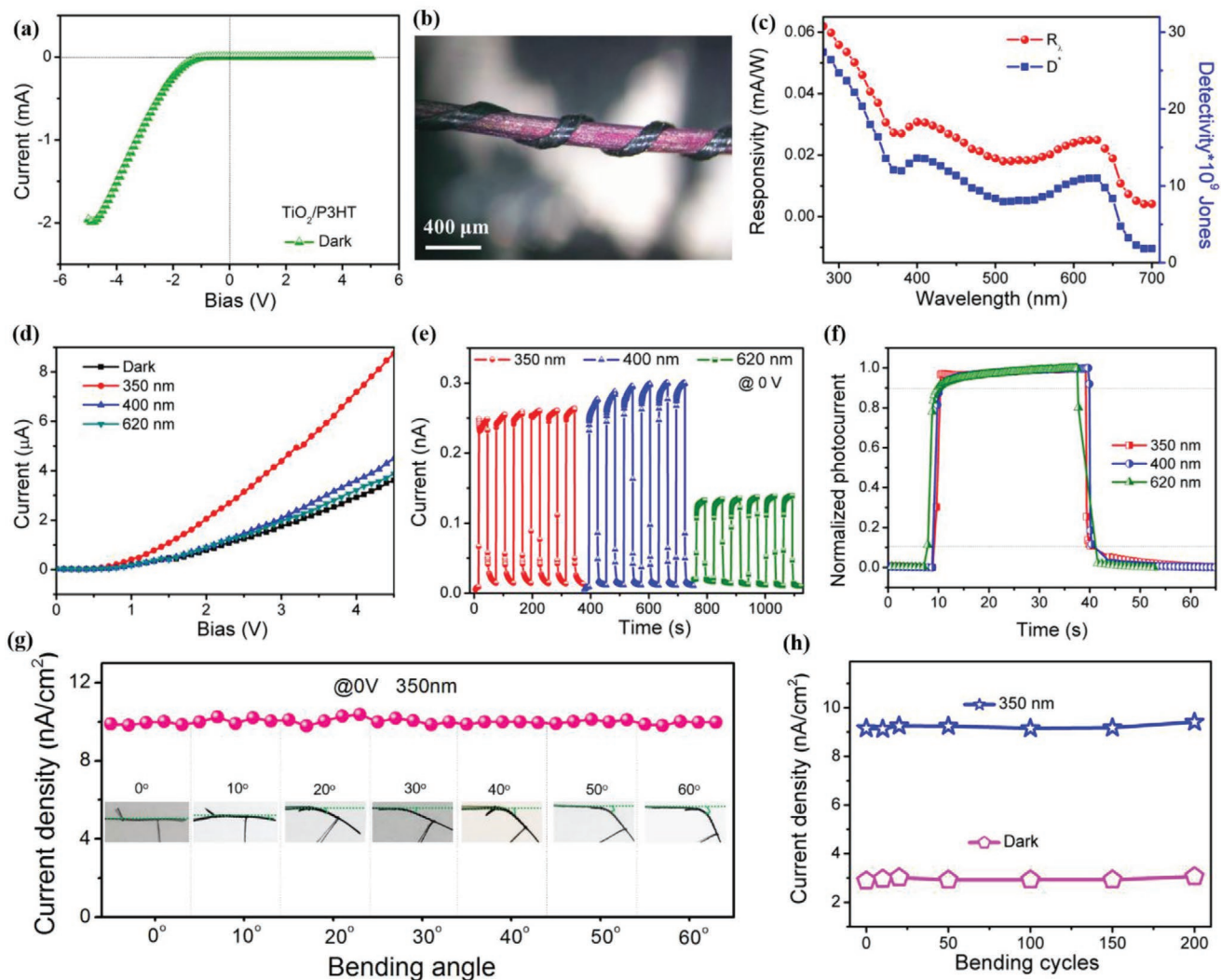**Figure 4.** Photoelectric properties of self-powered TiO_2/P3HT FPD. a) $I–V$ curve in the dark. b) Optical photograph of the device. c) Responsivity and detectivity as a function of wavelengths at zero bias. d) $I–V$ curves and e) $I–t$ curves. f) Normalized $I–t$ curves in one cycle. g) Photocurrent density upon different bending angles from 10° to 60° at zero bias, insets show the corresponding device photos. h) Photocurrent tests after 200 bending cycles at 60°.

an obvious rectification characteristic with a ratio of 567 at ±4 V, suggesting the typical photodiode behavior (Figure 4a). By comparison, the symmetric I–V curve under dark for pure TiO_2NTs FPD indicates that the heterojunction between CNT yarn electrode and TiO_2 can be negligible and unable to induce self-powered property (Figure S3, Supporting Information). While the linear I–V curve under dark for pure P3HT device (Figure S4, Supporting Information) reveals good ohmic contacts at CNT-P3HT-Ti and no photoresponse can be detected upon 365 and 450 nm light illumination. Thus, it is safe to confirm that the excellent rectifying feature of TiO_2/P3HT FPD originates from the p-n junction of p-P3HT/n-TiO_2, which is also the origin of self-powered photoresponse. The FPD device structure is displayed in Figure 4b where CNT yarn is intertwined tightly around the fibrous sample to ensure intimate and stable contact, beneficial for high charge collection efficiency. The spectral responsivity (R_λ) and detectivity (D^*) as a function of wavelength of the TiO_2/P3HT FPD working at self-powered mode are shown in Figure 4c, which are defined as the following equations.[10,23,38]

$$R_\lambda = \frac{I_{ph} - I_d}{PS} \tag{1}$$

$$D^* = \frac{R_\lambda}{(2eI_d/S)^{1/2}} \tag{2}$$

where I_{ph} is the photocurrent, I_d is the dark current, P is the light power density, S is the effective area under irradiation, and e is the electronic charge. An obvious high responsivity can be observed over a wide wavelength range from UV to visible (280–700 nm) region. Two dominant peaks are appeared in the visible range with values of 0.031 mA W^{-1} at 400 nm and 0.025 mA W^{-1} at 620 nm. In the UV region (280–390 nm), the R_λ values increase with shorter wavelengths and the calculated value at 350 nm is 0.037 mA W^{-1}. The detectivity reflects the device ability to detect weak signals from the noise environment. By assuming the shot noise from the dark current is the major contributor and calculating using Equation (2), the D^* values are 1.63×10^{10}, 1.61×10^{10}, and 1.09×10^{10} Jones under

0 V at wavelengths of 350 nm, 400 nm, and 620 nm, respectively. The performance of the as-prepared FPDs in this study is compared with previously reported flexible fibrous detectors (**Table 1**). It is shown that the detectivity up to 10^{10} Jones is obtained, which is nearly one order of magnitude higher than previously reported ZnO/Spiro-MeOTAD device[42] and comparable to CdS/P3HT wire device.[32]

Figure 4d,e demonstrate the I–V curves under dark and light illumination of 620, 400, and 350 nm, and current-time I–t curves at zero bias with repeated light-switching behavior of the self-powered broadband TiO_2/P3HT FPD. The photocurrent increases slightly under illumination of visible light (620 and 400 nm) while it increases dramatically under UV light, indicating a UV–visible broadband FPD, in consistent with the Responsivity spectra in Figure 4c. The on-off switching curve is reproducible and stable without notable photocurrent decay. The photocurrent values are found to be 0.25, 0.30 and 0.13 nA at 350 nm, 400 nm and 620 nm, respectively. Moreover, the FPD endows a fast response speed by normalizing the I–t curves in one cycle (Figure 4f). Both the rise (peak current increases from 10% to 90%) and fall times (peak current drops from 90% to 10%) are within several seconds (Figure S5, Supporting Information), and the rise time is even below 1 s. The rise and fall times are estimated to be 0.72 and 0.5 s, respectively, when using 350 nm light, which is also comparable to the recently reported self-powered TiO_2/CuZnS fiber-shaped device (Table 1)[10] The high responsivity/detectivity and fast response speed together with good stability promise great potential applications for self-powered flexible optoelectronic devices. Flexibility is another crucial parameter to evaluate the practicability of FPD in real-life. As shown in Figure 4g,h, the device shows an excellent stability with a stable photocurrent density of ≈10 nA cm^{-2} whilst being operated at bending angles from 10°,20°,30°,40°,50°,60° at zero bias under 350 nm illumination. In addition, both the dark and photo current densities remain unchanged when bending at 60° for repeating 200 times. It is possibly because the good adhesion of TiO_2 in situ grown on the surface of Ti wire, the intimate contact between CNT yarn electrode and TiO_2/P3HT hybrids and the highly flexible organic component (P3HT polymer) contribute

Table 1. Comparison of the critical parameters for fibrous photodetectors.

Device	Bias	Wavelength	Rise time	Fall time	Responsivity	Detectivity	Ref.
ZnO/PVK/graphene	−0.5 V	340 nm	0.28 s	2.2 s	900 mA W^{-1}		[14]
ZnO/PVK/PEDOT:PSS	−0.5 V	340 nm	6 s	7 s	120 mA W^{-1}		
ZnO/graphene	−2 V	325 nm	0.52 s	3.4 s	1.92 A W^{-1}		[20]
CdS/P3HT	0 V	780 nm	0.2 s	0.2 s	10.5 mA W^{-1}	6.64×10^{10} J	[32]
TiO_2/CuZnS	0 V	320 nm	<0.2 s	<0.2 s	≈2.1 mA W^{-1}		[10]
ZnO/PVK	0 V	350 nm	1.5 s	6 s	9.96 mA W^{-1}		[9]
Perovskite/CuO	0V	350 nm	<0.2 s	<0.2 s	126.3 mA W^{-1}	3.97×10^{12} J	[31]
ZnO/Spiro-MeOTAD	0 V	365 nm	0.16 s	0.2 s	0.8 mA W^{-1}	4.2×10^{9} J	[42]
TiO_2/P3HT	0 V	350 nm	0.72 s	0.5 s	0.037 mA W^{-1}	1.63×10^{10} J	This work
		400 nm	1.1 s	0.5 s	0.031 mA W^{-1}	1.61×10^{10} J	
		620 nm	1.4 s	3.1 s	0.025 mA W^{-1}	1.09×10^{10} J	
Au/TiO_2/P3HT	0 V	350 nm	0.48 s	2.12 s	0.25 mA W^{-1}	2.9×10^{10} J	

greatly to the overall superior stable performance under bending state, promising for wearable electronic devices.

The optical properties of TiO_2, P3HT, and TiO_2/P3HT hybrids are determined by the UV–visible diffuse reflectance spectra as displayed in **Figure 5**a, which can be used to explain the broadband responsivity of the flexible self-powered TiO_2/P3HT FPD. The TiO_2NTs sample exhibits intense spectral response in the UV range with a wavelength below 390 nm (peak at 365 nm), ascribing to the large energy bandgap of anatase TiO_2 (≈3.15 eV using Kubelka–Munk equation,[40] Figure 5b). The weak absorption in the visible light region (400–700 nm) is because of the light scattering effect caused by pores/cracks in the nanotubes.[38,43] While pure P3HT sample exhibits a broad and strong absorption from UV to visible region (350–650 nm) with a peak centered at ≈460 nm and the optical band gap value is calculated to be 1.82 eV (Figure 5b) Accordingly, the optical absorption for TiO_2/P3HT hybrid enhances greatly when the wavelength is shorter than 650 nm, suggesting a broadband light harvesting ability, which is in good agreement with the responsivity and detectivity spectra in Figure 4c. It can be deduced that P3HT coating layer plays a dominant role in the broadband photoresponse in the photovoltaic mode. The energy levels of TiO_2 and P3HT are studied to reveal the working mechanism of the flexible self-powered FPD (Figure 5c). The band edge positions of these two materials are obtained from Ultraviolet photoelectron spectroscopy (UPS) analysis (Figure S6, Supporting Information), which indicates a type II heterojunction of p-P3HT and n-TiO_2. The p-n heterojunction would change the band bending at the interface and give a built-in electric field for the effective separation of photogenerated electrons and holes in TiO_2 and P3HT. Driven by the electric field, holes drift from the valence band of TiO_2 to the highest occupied molecular orbital of P3HT and subsequently are collected by CNT yarn electrode (work function of 4.3 eV).[9] While photogenerated electrons in the TiO_2 are collected by the Ti metal electrode (work function of 4.33 eV). The P3HT acts as an electron blocking layer to impede the electrons transferring from TiO_2 to P3HT, which greatly reduces the carrier recombination. Noted that the fibrous device configuration allows charge carriers move along the longitudinal direction of the NTs and reach the inner Ti microwire electrode and outer CNT yarn electrode (Figure 5d), promising a more effective charge collection and higher photoresponse comparing with the traditional planar device.[10] As a result, with the high separation and transfer efficiency of photoinduced electrons and holes, obvious photoresponse is accomplished.

Furthermore, the photosensitivity property of the self-powered flexible broadband TiO_2/P3HT FPD was measured using a range of irradiances of 0–1 mW cm^{-2}. The photocurrent is steadily increasing with respect to the increased light intensity for all the three wavelengths as shown in **Figure 6**a–c, giving photocurrent values of 293 pA at 0.748 mW cm^{-2} at 350 nm, 336 pA at 0.927 mW cm^{-2} at 400 nm and 151 pA at 0.381 mW cm^{-2} at 620 nm. The phenomenon proves that the charge carrier photogeneration efficiency is proportional to the absorbed photon flux and the nonlinear relationship for the photocurrent variation against illuminance intensity can be fitted by the power law.[44]

$$I_{ph} = AP^{\theta} \qquad (3)$$

where A is a constant for a certain wavelength, and the exponent θ determines the photocurrent response to light intensity.
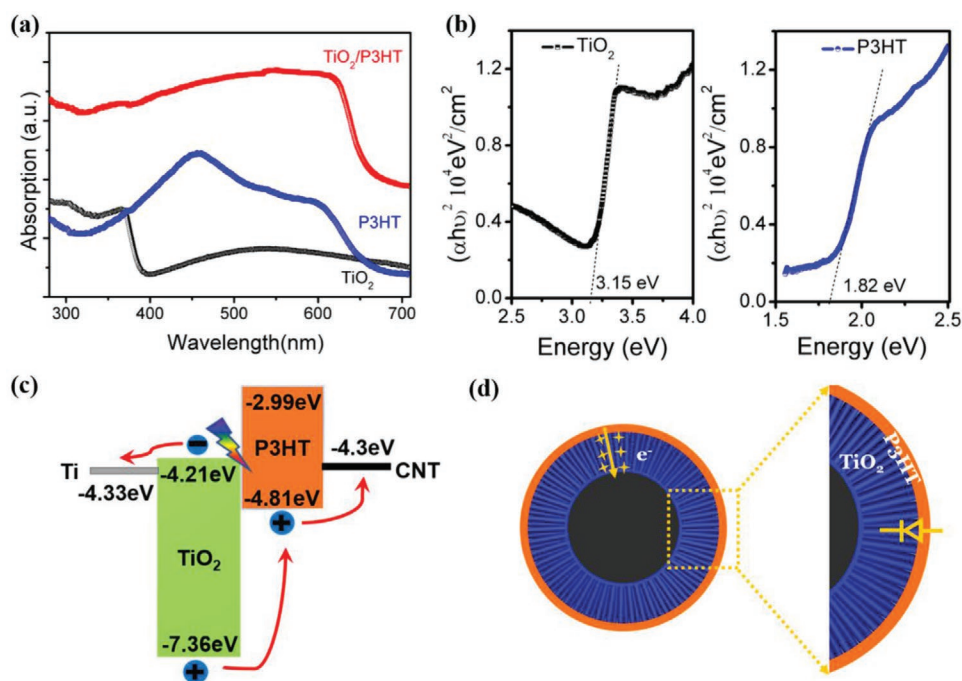
Figure 5. a) UV–vis diffuse reflectance spectra (DRS) of TiO_2, P3HT and TiO_2/P3HT hybrid. b) The Kubelka–Munk transformed spectra of TiO_2 and P3HT where the slops of the tangents on the horizontal axis refer to the bandgap energies. c) Energy level diagram of device. d) Schematic cross-sectional morphology of the device.
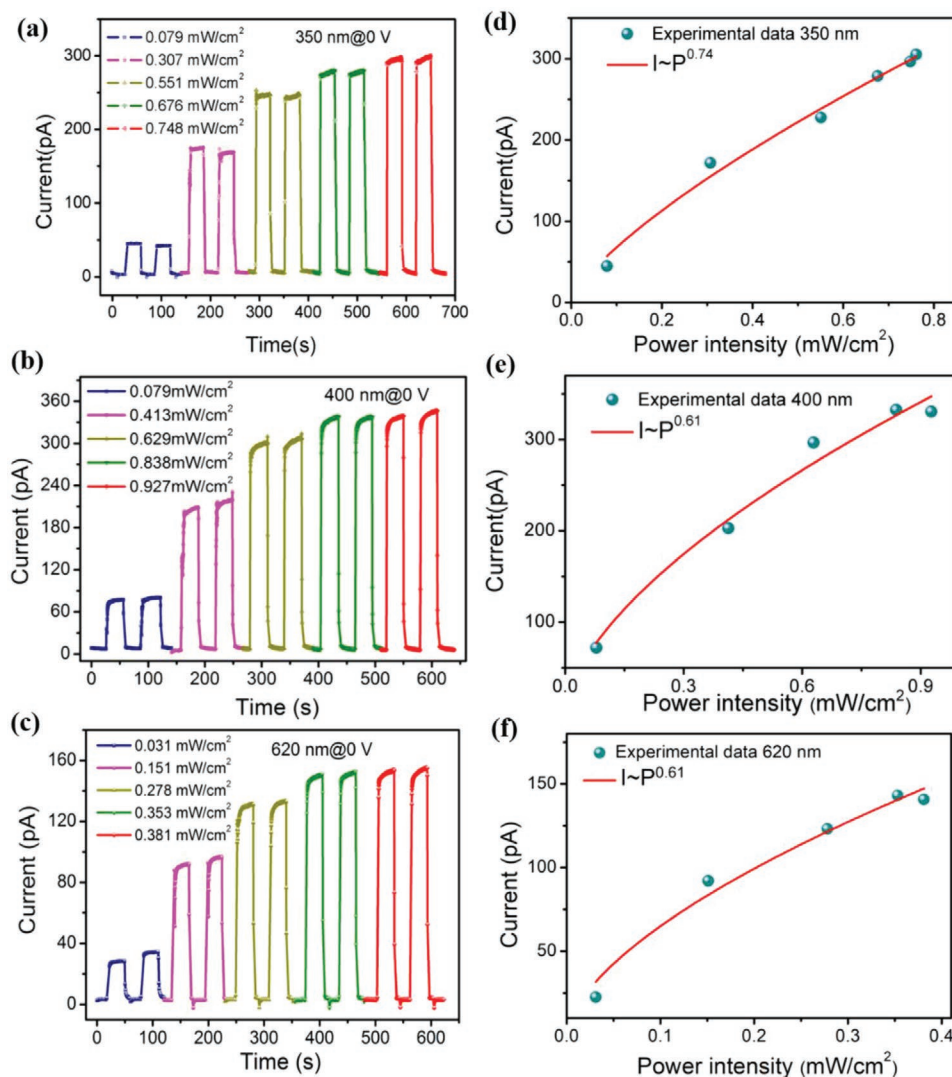
Figure 6. a–c) Time-dependent photocurrent response at zero bias for TiO$_2$/P3HT FPD upon light illumination of 350, 400, and 620 nm with varying light intensities, respectively, and d–f) their corresponding fitting curves for the relationship between the photocurrent and the light intensity.

Figure 6d–f display the fitting curves using equation (3) and the calculated values are 0.74, 0.61, and 0.61 at wavelengths of 350, 400, and 620 nm, respectively. Such a nonunity exponent (0.5 < θ < 1) suggests a rather complex process in the self-powered FPD including the generation, separation, recombination, and trapping of the electron-hole pairs.[21,24,45,46]

In order to further improve the photoelectric performance especially the responsivity of the self-powered flexible TiO$_2$/P3HT FPD, AuNPs were deposited on the surface of the composites by an ion sputtering method. **Figure 7** and **Table 2** show the comparison of photoelectric performance of TiO$_2$/P3HT FPD and four different Au/TiO$_2$/P3HT FPDs by controlling the Au deposition intervals from 15 to 60 s. The SEM images of the four Au/TiO$_2$/P3HT hybrids with size distribution of AuNPs are displayed in Figure S7, Supporting Information. With the increasing sputtering duration, both the size and density of AuNPs increase. The dark currents for different FPDs follow the trend: 60sAu/TiO$_2$/P3HT > 45sAu/TiO$_2$/P3HT > TiO$_2$/P3HT > 15sAu/TiO$_2$/P3HT > 30sAu/TiO$_2$/P3HT (Figure 7a),

indicating that a lower amount of AuNPs with discrete coverage leads to the suppression of dark current (15 and 30 s) while further increasing AuNPs with dense distribution (45 and 60 s) results in higher dark current comparing with the TiO$_2$/P3HT FPD counterpart without AuNPs deposition. The deposition of AuNPs leads to the formation of Schottky barriers,[46–48] which gradually decreases the concentration of charge carrier in the composite and results in the greatly reduce of dark currents. However, further increasing the sputtering time (45 and 60 s), the bigger and denser AuNPs lead to higher conductivity and thus higher dark currents. The dark current increases sharply (about 100 times higher than that of TiO$_2$/P3HT FPD) when the sputtering intervals increases from 30 to 45 s. The 30sAu/TiO$_2$/P3HT hybrid FPD exhibits the lowest dark currents under biases from 1 to 3 V (Inset in Figure 7a), and it was selected as the typical Au-modified self-powered flexible FPD for further investigation. When the UV light is on, the dramatically increased photocurrent of Au/TiO$_2$/P3HT FPDs (Figure S8, Supporting Information) is possibly due to the hot electron
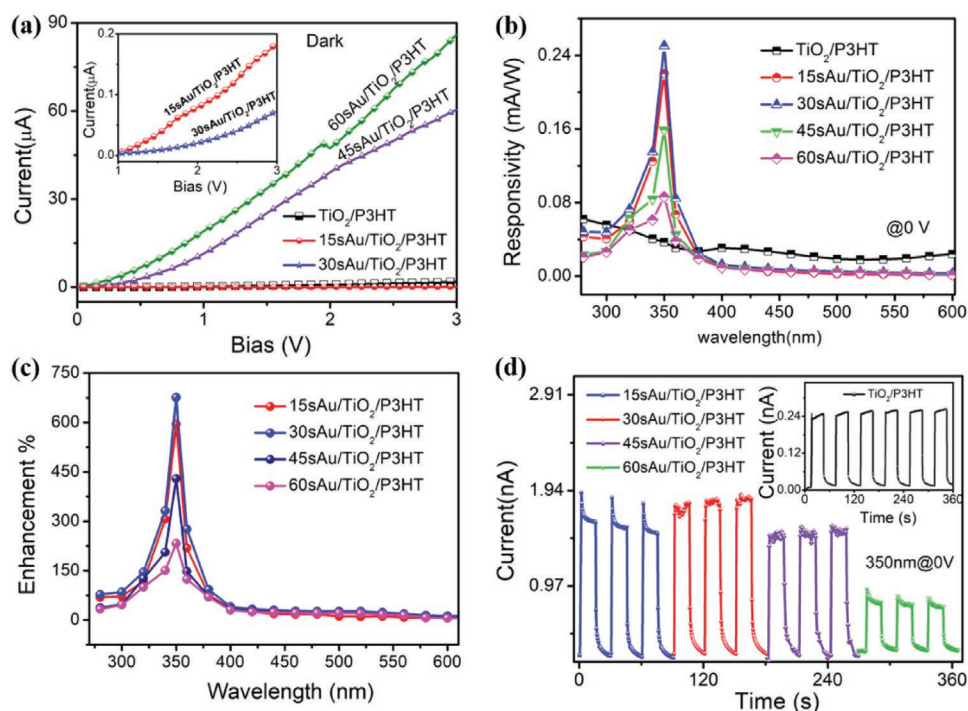
Figure 7. Comparison of photoelectric properties of TiO_2/P3HT FPD and Au/TiO_2/P3HT FPDs. a) I–V curves under dark, b) responsivity spectra at zero bias, and c) responsivity enhancement compared with TiO_2/P3HT FPD. d) I–t curve at zero bias under 350 nm illumination. Insets in a,d) show the enlarged I–V curves, and I–t curve, respectively.

injection effect of AuNPs.[48–50] Surprisingly, all the four Au/TiO_2/P3HT FPDs can work under self-powered mode and show dramatically enhanced responsivity within UV range (320–380 nm) with a peak at 350 nm and decreased values in the visible range (400–600 nm) compared with the TiO_2/P3HT FPD at zero bias (Figure 7b,c). The related photoelectric performances are listed in Table 2. The UV–visible rejection ratios (R_{350nm}/R_{400nm}) are calculated to be ≈20 for 15sAu/TiO_2/P3HT and 30sAu/TiO_2/P3HT FPDs, ≈17 times higher than that of TiO_2/P3HT FPD (≈1.2). The sharp cut-off edge and high UV–visible rejection ratio suggest high photosensitivity and selectivity, indicating that the Au/TiO_2/P3HT FPD is a high-performance self-powered UV photodetector. The I–t curves with on-off switching upon 350 nm light illumination at zero bias are shown in Figure 7d, which examines the effect of tailored AuNPs on the self-powered property. The highest photocurrent values are found on 30sAu/TiO_2/P3HT hybrid FPD with a value of ≈1.9 nA, which is 7.5 times higher than that of TiO_2/P3HT FPD (Table 2). The rise times for all the Au/TiO_2/P3HT hybrid FPDs are within 1 s and fall times are a few

seconds, indicating fast response speed for the self-powered flexible FPDs after AuNPs decoration.

To get more insight into the AuNPs enhancement effect, 30sAu/TiO_2/P3HT FPD was chosen for more investigation, and the results are presented in **Figure 8**. The I–V curves under dark and 350 nm illumination are shown in Figure 8a, which indicates typical photodiode behavior and obvious self-powered feature. Comparing the I–V curves in the dark and 350 nm light of 30sAu/TiO_2/P3HT FPD and TiO_2/P3HT FPD (Figure S9, Supporting Information), it can be easily observed that the dark currents decrease greatly and photocurrents increase largely for AuNPs modified device, leading to photoresponse boost. The responsivity at 0 V increases largely within UV range (320–380 nm) with a peak value of 0.25 mA W^{-1} at 350 nm for 30sAu/TiO_2/P3HT FPD (Figure 8b), which can be explained by the light absorption property (Figure S10, Supporting Information). The 30sAu/TiO_2/P3HT composite exhibits strong light absorption ability in the UV range with a wavelength below 390 nm. The maximum responsivity is nearly 700% enhancement compared to that of TiO_2/P3HT FPD. In the dark, the

Table 2. Summary of the characteristic parameters of self-powered TiO_2/P3HT FPD and different Au/TiO_2/P3HT FPDs in this study.

Device	Dark current [I_d]	Photo current [I_{ph}]	Rise/fall times	$R_{350\ nm}$ [0 V]	UV–vis rejection ratio [R_{350}/R_{400}]	R_{350} enhancement
TiO_2/P3HT	0.015 nA	0.252 nA	0.72/0.50 s	37.0 µA W^{-1}	1.20	–
15sAu/TiO_2/P3HT	0.267 nA	1.652 nA	0.64/1.16 s	220.3 µA W^{-1}	20.08	595%
30sAu/TiO_2/P3HT	0.286 nA	1.857 nA	0.48/2.12 s	250.3 µA W^{-1}	20.12	676%
45sAu/TiO_2/P3HT	0.319 nA	1.504 nA	0.93/4.53 s	158.9 µA W^{-1}	15.50	429%
60sAu/TiO_2/P3HT	0.335 nA	0.792 nA	0.68/1.05 s	86.2 µA W^{-1}	9.14	233%
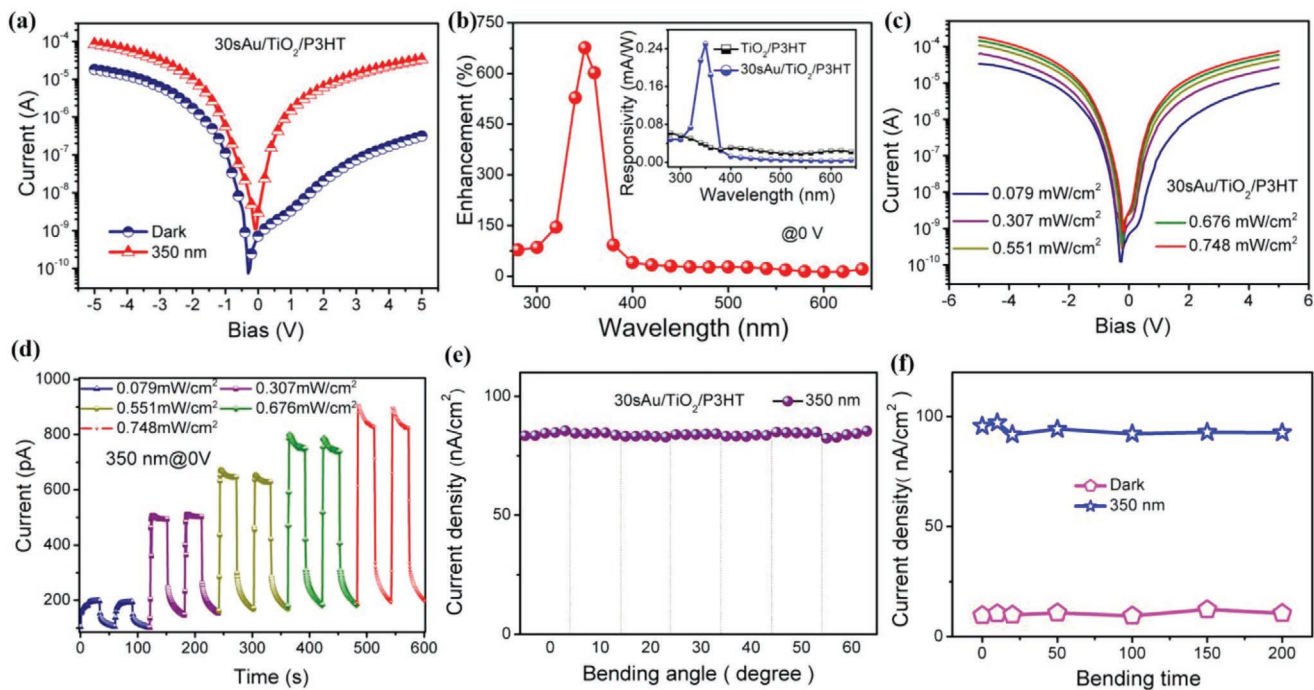
Figure 8. Photoelectric properties of self-powered 30sAu/TiO_2/P3HT FPD. a) I–V curves under dark and 350 nm illumination. b) Responsivity enhancement at zero bias compared with TiO_2/P3HT FPD. Inset shows the responsivity spectra. c) I–V and d) I–t curves under 350 nm illumination with different light intensities. e) Photocurrent density upon different bending angles from 10° to 60° at 0 V and f) photocurrent tests after 200 bending times at 60°.

formation of Schottky barriers after AuNPs deposition will gradually decreases the concentration of charge carrier and results in decreased dark currents.[46–48] Upon UV light illumination, hot electrons with a wide energy distribution range between 1 and 4 eV primarily generate through the intraband transitions in AuNPs considering their interband transition threshold from the d band to s band is ≈2.4 eV.[51–53] Hot electrons with energies larger than the Schottky barrier at the Au–TiO_2 interface will be injected into the conduction band (CB) of TiO_2 and then collected by the Ti metal electrode. It will result in the increase of total concentration of electrons in the Au/TiO_2/P3HT system and thereby enhancing the photocurrent/responsivity. While under visible light illumination, only P3HT could generate electron-hole pairs and the Schottky barriers formed between AuNPs and P3HT will block the carrier transportation, which promotes the fast decay of the current, resulting in decreased photocurrent in visible range and slow fall times.[48] Moreover, the optical sensitivity and flexibility performance of 30sAu/TiO_2/P3HT FPD device at 350 nm is shown in Figure 8c–f. With the increase of light intensity, the photocurrent increases steadily, giving photocurrent values of 196 pA at 0.079 mW cm^{-2}, 502 pA at 0.307 mW cm^{-2}, 647 pA at 0.551 mW cm^{-2}, 762 pA at 0.676 mW cm^{-2}, and 856 pA at 0.748 mW cm^{-2}. The exponent of the nonlinear relationship for the variation of photocurrent against irradiance intensity is about 0.67 (Figure S11, Supporting Information) using Equation (3). The above results indicate that optimal Au NPs decoration can boost the overall photodetection performance including responsivity, selectivity, and sensitivity. In addition, highly stable photocurrent density with a value of ≈84 nA cm^{-2}

at 0 V are observed at bending 0–60° and both the photocurrent and dark current remain unchanged at 60° bending angles after repeating 200 times, further verifying the excellent flexibility of the hybrid FPD device.

3. Conclusion

In summary, a novel flexible inorganic-organic UV–visible broadband TiO_2/P3HT FPD is successfully constructed with good self-powered property and high stability photodetection during device deformation. Surprisingly, the photoresponsivity and selectivity are dramatically enhanced after AuNPs decoration, enabling a high-performance self-powered fiber-shaped UV photodetector, which shows great potential for future wearable electronic devices. The optimal 30sAu/TiO_2/P3HT FPD shows ≈700% responsivity enhancement under UV light illumination, and ≈1700% higher UV–visible rejection ratio (R_{350}/R_{400}) at 0 V compared with the counterpart device without AuNPs. The present work might shed light on the optimization of flexible optoelectronic devices with improved self-powered property.

4. Experimental Section

Synthesis of TiO_2NTs: The Ti microwires (99.6%, ≈200 μm) were ultrasonically cleaned in acetone, ethanol, and deionized water successively, and then dried in a nitrogen stream before anodization. Anodic TiO_2NTs were generated in a two-electrode cell with a mixture of NH_4F (0.36 wt%) and H_2O (2 wt%) in the ethylene glycol as the

electrolyte. The Ti wire was used as the anode and Pt gauze as the cathode. A conventional two-step anodization method was used to grow highly-ordered TiO$_2$NTs on the Ti wire. The Ti wire was first anodized at 60 V for 2 h, and the formed oxide film was removed by sonication in ethanol. Then the Ti wire was anodized for a second time under the same condition except for a short duration (10 min). Afterward, the anodized wire was washed with ethanol and deionized water for several times, and then dried with N$_2$, followed by an annealing process in ambient air at 450 °C for 2 h to generate anatase Ti-TiO$_2$NTs

Synthesis of TiO$_2$/P3HT Hybrid: The synthesized Ti-TiO$_2$NTs sample was transferred to a glass-bottle and then sealed to undergo a vacuum treatment for 2h. P3HT (Regioregular polymer, Aladdin) with a concentration of 10 mg mL^{-1} in chlorobenzene solution was injected into the bottle and then kept it in vacuum for another 2 h to fabricate TiO$_2$/P3HT Hybrid. Then the sample was taken out quickly and thermally treated at 150 °C in a vacuum oven for 30 min for a better electrical conductivity as well as removing the residues.

Synthesis of Au/TiO$_2$/P3HT Hybrid: AuNPs were deposited on TiO$_2$/P3HT hybrid samples by a simple ion sputtering method. The fibrous sample was put into the chamber of the equipment which was then under a vacuum treatment until the pressure reached 0.15 mbar. The sputtering process was carried out at a current of 6 mA with different durations. After sputtering, the pressure was recovered and the Au deposited samples were taken out for device fabrication.

Synthesis of CNT Yarn: The CNT yarn was made by chemical vapor deposition spinning method from ethanol/acetone carbon source with ferrocene as catalyst and thiophene promoter in hydrogen flow at 1250 °C.

Characterization: The morphology and microstructure of these hybrids were characterized by using a SEM (ZEISS GeminiSEM, Germany) and a HRTEM (JEOL JEM200CX, JEOL). Powder XRD (Bruker D8 Advance diffractometer with Cu-Kα radiation) experiments were performed to study the crystallographic information. Raman spectroscopy (Renishaw invia Raman microscope) was performed using optical maser with 532 nm laser. UPS was measured with a monochromatic He I light source (21.2 eV) and a VG Scienta R4000 analyzer. The UV–vis diffuse reflectance spectra of the samples were recorded on a UV2700 type spectrophotometer (SHIMADZU).

Device Fabrication and Photoelectric Measurements: To assemble a fibrous photodetector, one end of Ti microwire was polished with sandpaper to expose the Ti metal, which acted as the inner electrode. CNT yarn was carefully twisted and winded around the photoactive material and the extended part acted as the outer electrode. The effective fiber length was fixed at 0.5 cm for each sample. The optoelectronic properties were collected with a semiconductor characterization system (Keithley 4200-SCS) and a 70 W xenon arc lamp with a monochromator was used as light source. The light intensity was measured with a NOVA II power meter (OPHIR photonics). All the measurements were performed at room temperature.

Supporting Information

Supporting Information is available from the Wiley Online Library or from the author.

Acknowledgements

Conflict of Interest

The authors declare no conflict of interest.

[1] S. Cai, X. Xu, W. Yang, J. Chen, X. S. Fang, *Adv. Mater.* **2019**, *31*, 1808138.
[2] D. Son, J. Kang, O. Vardoulis, Y. Kim, N. Matsuhisa, J. Y. Oh, J. W. F. To, J. Mun, T. Katsumata, Y. Liu, A. F. McGuire, M. Krason, F. Molina-Lopez, J. Ham, U. Kraft, Y. Lee, Y. Yun, J. B. H. Tok, Z. Bao, *Nat. Nanotechnol.* **2018**, *13*, 1057.
[3] C. Larson, B. Peele, S. Li, S. Robinson, M. Totaro, L. Beccai, B. Mazzolai, R. Shepherd, *Science* **2016**, *351*, 1071.
[4] A. Miyamoto, S. Lee, N. F. Cooray, S. Lee, M. Mori, N. Matsuhisa, H. Jin, L. Yoda, T. Yokota, A. Itoh, *Nat. Nanotechnol.* **2017**, *12*, 907.
[5] J. Kim, M. Kim, M.-S. Lee, K. Kim, S. Ji, Y.-T. Kim, J. Park, K. Na, K.-H. Bae, H. Kyun Kim, F. Bien, C. Young Lee, J.-U. Park, *Nat. Commun.* **2017**, *8*, 14997.
[6] E. Boto, N. Holmes, J. Leggett, G. Roberts, V. Shah, S. S. Meyer, L. D. Muñoz, K. J. Mullinger, T. M. Tierney, S. Bestmann, G. R. Barnes, R. Bowtell, M. J. Brookes, *Nature* **2018**, *555*, 657.
[7] M. D. Lima, R. H. Baughman, *Science* **2011**, *331*, 51.
[8] K. Cherenack, C. Zysset, T. Kinkeldei, N. Münzenrieder, G. Tröster, *Adv. Mater.* **2010**, *22*, 5178.
[9] Y. Dong, Y. Zou, J. Song, Z. Zhu, J. Li, H. Zeng, *Nano Energy* **2016**, *30*, 173.
[10] X. Xu, J. Chen, S. Cai, Z. Long, Y. Zhang, L. Su, S. He, C. Tang, P. Liu, H. Peng, X. S. Fang, *Adv. Mater.* **2018**, *30*, 1803165.
[11] S. J. Kim, M.-A. Kang, I.-S. Jeon, S. Ji, W. Song, S. Myung, S. S. Lee, J. Lim, K.-S. An, *J. Mater. Chem. C* **2017**, *5*, 12354.
[12] S. Y. Li, Y. Zhang, W. Yang, H. Liu, X. S. Fang, *Adv. Mater.* **2020**, *32*, 1905443.
[13] D. Ding, H. Li, H. Yao, L. Liu, B. Tian, C. Su, Y. Wang, Y. Shi, *J. Mater. Chem. C* **2019**, *7*, 9496.
[14] Z. Zhu, D. Ju, Y. Zou, Y. Dong, L. Luo, T. Zhang, D. Shan, H. Zeng, *ACS Appl. Mater. Interfaces* **2017**, *9*, 12092.
[15] M. Liao, L. Sang, T. Teraji, M. Imura, J. Alvarez, Y. Koide, *Jpn. J. Appl. Phys.* **2012**, *51*, 0115.
[16] T. Yang, S. Chen, X. Li, X. Xu, F. Gao, L. Wang, J. Chen, W. Yang, X. Hou, X. S. Fang, *Adv. Funct. Mater.* **2019**, *29*, 1806250.
[17] Y. Zhang, S. Li, W. Yang, M. K. Joshi, X. S. Fang, *J. Phys. Chem. Lett.* **2019**, *10*, 2400.
[18] D. Gedamu, I. Paulowicz, S. Kaps, O. Lupan, S. Wille, G. Haidarschin, Y. K. Mishra, R. Adelung, *Adv. Mater.* **2014**, *26*, 1541.
[19] Y. H. Ko, G. Nagaraju, J. S. Yu, *Nanoscale* **2015**, *7*, 2735.
[20] Z. Zhu, S. Wang, Y. Zhu, X. Liu, Y. Zou, Y. Gu, D. Ju, H. Zeng, *Adv. Mater. Interfaces* **2018**, *5*, 1800136.
[21] H. Fang, C. Zheng, L. Wu, Y. Li, J. Cai, M. Hu, X. S. Fang, R. Ma, Q. Wang, H. Wang, *Adv. Funct. Mater.* **2019**, *29*, 1809013.
[22] L. Zheng, F. Teng, Z. Zhang, B. Zhao, X. S. Fang, *J. Mater. Chem. C* **2016**, *4*, 10032.
[23] L. Zheng, P. Yu, K. Hu, F. Teng, H. Chen, X. S. Fang, *ACS Appl. Mater. Interfaces* **2016**, *8*, 33924.
[24] P. Yu, K. Hu, H. Chen, L. Zheng, X. S. Fang, *Adv. Funct. Mater.* **2017**, *27*, 1703166.
[25] Y. Ning, Z. Zhang, F. Teng, X. S. Fang, *Small* **2018**, *14*, 1703754.
[26] H. Chen, K. Liu, L. Hu, A. A. Al-Ghamdi, X. S. Fang, *Mater. Today* **2015**, *18*, 493.
[27] L. Su, W. Yang, J. Cai, H. Chen, X. S. Fang, *Small* **2017**, *13*, 1701687.

[28] H. Lu, W. Tian, F. Cao, Y. Ma, B. Gu, L. Li, *Adv. Funct. Mater.* **2016**, *26*, 1296.

[29] Z. Wang, J. Cheng, H. Huang, B. Wang, *Energy Storage Mater.* **2020**, *24*, 255.

[30] S. Bai, Q. Xu, L. Gu, F. Ma, Y. Qin, Z. L. Wang, *Nano Energy* **2012**, *1*, 789.

[31] H. Sun, W. Tian, F. Cao, J. Xiong, L. Li, *Adv. Mater.* **2018**, *30*, 1706986.

[32] X.-X. Yu, H. Yin, H.-X. Li, W. Zhang, H. Zhao, C. Li, M.-Q. Zhu, *Nano Energy* **2017**, *34*, 155.

[33] X. Wang, W. Song, B. Liu, G. Chen, D. Chen, C. Zhou, G. Shen, *Adv. Funct. Mater.* **2013**, *23*, 1202.

[34] X. Zhang, J. Li, W. Yang, B. Leng, P. Niu, X. Jiang, B. Liu, *ACS Appl. Mater. Interfaces* **2019**, *11*, 24459.

[35] D. Zhang, W. Zheng, R. Lin, Y. Li, F. Huang, *Adv. Funct. Mater.* **2019**, *29*, 1900935.

[36] K. Zhang, Z. L. Wang, Y. Yang, *ACS Nano* **2016**, *10*, 10331.

[37] J. Xu, W. Yang, H. Chen, L. Zheng, M. Hu, Y. Li, X. S. Fang, *J. Mater. Chem. C* **2018**, *6*, 3334.

[38] L. Zheng, K. Hu, F. Teng, X. S. Fang, *Small* **2017**, *13*, 1602448.

[39] L. Zheng, T. Feng, X. Ye, H. Zheng, X. S. Fang, *Adv. Energy Mater.* **2020**, *10*, 1902355.

[40] L. Zheng, S. Han, H. Liu, P. Yu, X. S. Fang, *Small* **2016**, *12*, 1527.

[41] W. C. Tsoi, D. T. James, K. Jong Soo, P. G. Nicholson, C. E. Murphy, D. D. C. Bradley, N. Jenny, K. Ji-Seon, *J. Am. Chem. Soc.* **2011**, *133*, 9834.

[42] Y. Shen, X. Yan, H. Si, P. Lin, Y. Liu, Y. Sun, Y. Zhang, *ACS Appl. Mater. Interfaces* **2016**, *8*, 6137.

[43] G. Li, Z. Lian, W. Wang, D. Zhang, H. Li, *Nano Energy* **2016**, *19*, 446.

[44] Q. Hong, Y. Cao, J. Xu, H. Lu, J. He, J. L. Sun, *ACS Appl. Mater. Interfaces* **2014**, *6*, 20887.

[45] L. Hui, Z. Zhang, L. Hu, G. Nan, L. Sang, M. Liao, R. Ma, F. Xu, X. S. Fang, *Adv. Opt. Mater.* **2015**, *2*, 771.

[46] H. Y. Chen, K. W. Liu, X. Chen, Z. Z. Zhang, M. M. Fan, M. M. Jiang, X. H. Xie, H. F. Zhao, D. Z. Shen, *J. Mater. Chem. C* **2014**, *2*, 9689.

[47] K. W Liu, M. Sakurai, M. Y. Liao, M. Aono, *J. Phys. Chem. C* **2010**, *114*, 119835.

[48] W. Ouyang, F. Teng, M. Jiang, X. S. Fang, *Small* **2017**, *133*, 1702177.

[49] Y. Fang, Y. Jiao, K. Xiong, R. Ogier, Z.-J. Yang, S. Gao, A. B. Dahlin, M. Käll, *Nano Lett.* **2015**, *15*, 4059.

[50] S. Noothongkaew, J. K. Han, Y. B. Lee, O. Thumthan, K.-S. An, *Prog. Nat. Sci.: Mater. Int.* **2017**, *27*, 641.

[51] S. Linic, P. Christopher, D. B. Ingram, *Nat. Mater.* **2011**, *10*, 911.

[52] A. Manjavacas, J. G. Liu, V. Kulkarni, P. Nordlander, *ACS Nano* **2014**, *8*, 7630.

[53] X. C. Ma, Y. Dai, L. Yu, B.-B. Huang, *Light: Sci. Appl.* **2016**, *5*, e16017.

2001604 (11 of 11)